KALMAN FILTERING AND ATMOSPHERIC PREDICTABILITY*

Martin Ehrendorfer
Institute for Meteorology and Geophysics, University of Vienna
Vienna, Austria

1. INTRODUCTION AND MOTIVATION

Preliminary results obtained with an exact low–resolution Extended Kalman Filter (EKF) based on quasigeostrophic (QG) dynamics are described. These results concern primarily the assessment of the analysis error covariance matrix, $\mathbf{P}^a$, through the EKF, as well as some implications for atmospheric predictability and data assimilation resulting from knowledge of $\mathbf{P}^a$.

The development of an EKF is motivated both in a predictability and in a data assimilation context. In both contexts, $\mathbf{P}^a$ is of primary importance. In the predictability context, knowledge of $\mathbf{P}^a$ allows for the computation of singular vectors (SVs), denoted $\mathbf{Z}_0$, as the solution of the following generalized eigenproblem:

$$\mathbf{P}^a\mathbf{M}_\tau^{\mathrm{T}}\mathbf{C}^{\mathrm{T}}\mathbf{C}\mathbf{M}_\tau\mathbf{Z}_0 = \mathbf{Z}_0\Lambda \qquad \text{with} \qquad \mathbf{Z}_0^{\mathrm{T}}(\mathbf{P}^a)^{-1}\mathbf{Z}_0 = \mathbf{I}\,, \tag{1.1}$$

where $\mathbf{M}_\tau$ denotes the tangent–linear model resolvent over the optimization time τ, $\mathbf{C}^{\mathrm{T}}\mathbf{C}$ denotes a norm to measure the model state (at final time), Λ denotes the diagonal (real) eigenvalue matrix, and $\mathbf{Z}_0$ is the set of (initial–time) SVs. Given that the set of SVs $\mathbf{Z}_0$ satisfies (1.1), their time–evolved counterparts (i.e., $\mathbf{C}\mathbf{M}_\tau\mathbf{Z}_0$) are the eigenvectors of the (tangent–linearly approximated) forecast error covariance matrix (see, e.g., Ehrendorfer and Tribbia 1997). Note that this property is inherently linked to knowledge of $\mathbf{P}^a$ in the computation (1.1); consequently, the SVs computed according to (1.1) must be considered to be of primary importance in an ensemble prediction context (e.g., in the process of generating perturbations valid at the initial time; see also, section 3.3, and Palmer et al. 1998).

In a data assimilation context, the short–term (e.g., 6 hours) time evolution of $\mathbf{P}^a$, namely, the forecast error covariance matrix, denoted $\mathbf{P}^f$, represents a flow–dependent formulation of the background error covariances, generically denoted as $\mathbf{B}$, that must be specified in the variational data assimilation context. In such variational assimilation schemes it is attempted to minimize a cost function $J(\mathbf{x})$ expressed here in the three–dimensional variational (3DVAR) context as:

$$J(\mathbf{x}) = \frac{1}{2}(\mathbf{x}-\mathbf{x}^b)^{\mathrm{T}}(\mathbf{P}^f)^{-1}(\mathbf{x}-\mathbf{x}^b) + \frac{1}{2}(\mathbf{H}\mathbf{x}-\mathbf{y}^o)^{\mathrm{T}}\mathbf{R}^{-1}(\mathbf{H}\mathbf{x}-\mathbf{y}^o)\,, \tag{1.2}$$

through variation of the model state vector $\mathbf{x}$. Here $\mathbf{x}^b$ represents the background (or, first guess) fields, $\mathbf{H}\mathbf{x}$ is the model analog for the observations $\mathbf{y}^o$ (linear observation operator), and $\mathbf{R}$ represents the observational error covariances. Note that J is the sum of a background term and an observational term. The specification of the background error covariances $\mathbf{B}$ is a difficult procedure in a variational data assimilation context; however, the flow–dependent $\mathbf{P}^f$ may be used in J, as indicated in (1.2) to replace $\mathbf{B}$, as $\mathbf{P}^f$ is provided in a natural way from $\mathbf{P}^a$ when the EKF equations are implemented.

2. IMPLEMENTATION OF THE EKF

The distinguishing feature of the EKF described here is that the second–order equations (for analysis and forecast error covariances) of the EKF are implemented without approximations (see, Epstein 1969, for the closely related stochastic dynamic equations). Such an exact implementation is (in view of the size of matrices involved) only possible at a rather low model resolution. The model resolution chosen here is T21 with three (pressure) levels in the vertical (i.e., T21L3). In addition, the prediction step is carried out with QG dynamics. Consequently, the filter is referred to as QG/EKF. For implementations of the EKF with more comprehensive dynamics (or better resolution), but approximated EKF equations, reference is made to Fisher (1998), Rabier et al. (1997), Houtekamer and Mitchell (1998), and Burgers et al. (1998) (see also, Todling et al. 1998).

The second–order EKF equation to determine the analysis error covariance matrix $\mathbf{P}^a$ is given by (analysis step):

$$\mathbf{P}^a(t_i) = \left(\mathbf{I}-\mathbf{K}_i\mathbf{H}_i\right)\overbrace{\mathbf{P}^f(t_i)} = \left([\mathbf{P}^f(t_i)]^{-1} + \mathbf{H}_i^{\mathrm{T}}(\mathbf{R}_i)^{-1}\mathbf{H}_i\right)^{-1}, \tag{2.1}$$

where the meaning of the matrices is the same as in section 1, and $\mathbf{K}_i$ is the *Kalman gain* matrix (see below). The incoming arrow in (2.1) indicates that in the computation (2.1) it is indeed the dynamically–predicted

*To appear in Proceedings ECMWF Workshop on Diagnosis of Data Assimilation Systems, European Centre for Medium–Range Weather Forecasts, Reading, England, UK, 2–4 November 1998.

forecast error covariance matrix $\mathbf{P}^f$ that is used. In the QG/EKF, eq. (2.1) is computed within the 3DVAR configuration of the ECMWF Integrated Forecasting System (IFS) through the second derivative of the cost function J which allows one to use the operationally available observations (for details, see, Ehrendorfer and Bouttier 1998a, b). In the prediction step, $\mathbf{P}^a$ is evolved tangent–linearly into $\mathbf{P}^f$ according to:

$$\underbrace{\mathbf{P}^f(t_{i+1})}_{\Downarrow} = \mathbf{M}_i \mathbf{P}^a(t_i) \mathbf{M}_i^{\mathrm{T}} + \mathbf{Q}(t_{i+1}) \,, \tag{2.2}$$

where, in the specific situation of the QG/EKF, $\mathbf{M}$ denotes the tangent–linear QG model described by Marshall and Molteni (1993). The $\mathbf{Q}$–term in (2.2) represents the effect of model error. The outgoing arrow indicates that the result of (2.2) is used in (2.1) as input, thus closing the loop. For completeness, two equivalent expressions for the Kalman gain are given as:

$$\mathbf{K}_i = \mathbf{P}^f(t_i) \mathbf{H}_i^{\mathrm{T}} \left(\mathbf{H}_i \mathbf{P}^f(t_i) \mathbf{H}_i^{\mathrm{T}} + \mathbf{R}_i \right)^{-1} = \mathbf{P}^a(t_i) \mathbf{H}_i^{\mathrm{T}} (\mathbf{R}_i)^{-1} \,. \tag{2.3}$$

For the detailed derivation of eqs. (2.1)–(2.3), as well as the corresponding first–order equations, reference is made to the excellent articles by Courtier (1997) and Cohn (1997) (see also, Ide et al. 1997). Details on the 3DVAR implementation at ECMWF may be found in Courtier et al. (1998).

3. SELECTED PRELIMINARY RESULTS

Results are presented here for a continuous assimilation experiment with the QG/EKF over a period of several days starting at 19971128/00 GMT. During this assimilation experiment, conventional observations were used at 6–hour intervals. During the first day, the EKF prediction step was performed without model error; however, after this initial period a simple model error formulation was used in order to prevent the analysis error variances from approaching zero. The basic result of this experiment is a time sequence of analysis and background error covariance matrices (in terms of vorticity), $\mathbf{P}_\zeta^a$ and $\mathbf{P}_\zeta^f$. Some of these matrices are discussed in the following (basic properties; section 3.1), and diagnosed with regard to SVs (section 3.2), ensemble integrations and predictability (section 3.3), and their structure in the IFS control variable space (section 3.4). More details about this experiment may be found in Ehrendorfer and Bouttier (1998b).

3.1 THE ANALYSIS ERROR COVARIANCE MATRIX

Fig. 1 shows the vorticity *variances* of the analysis error covariance matrix $\mathbf{P}_\zeta^a$ valid for 19971201/00 GMT, in physical space for the three model levels. The impact of observations is reflected by decreased variances over North America, Europe, and Australia. The analysis error variances are largest in the top model layer, decreasing downward. The total (vorticity) analysis error variance is in this situation 1.0449×10^{-11} s^{-2}, distributed over the levels as 6.12×10^{-11} s^{-2} at 200 hPa, 3.38×10^{-11} s^{-2} at 500 hPa, and 0.94×10^{-11} s^{-2} at 800 hPa. It is also interesting to note that the magnitude of these variance fields in physical space is (in an overall root–mean–square sense) approximately 10^{-10} s^{-2} which seems a reasonable analysis error *variance* level for (relative) vorticity.

It is of interest to study the spectral decomposition of the analysis error variances. Since the QG/EKF formulation is in spectral form (triangular truncation), it is natural to consider the quantity $\mathcal{Q}$ in the form:

$$\mathcal{Q} = \sum_{l=1}^{3} \sum_{n=0}^{N} \underbrace{\sum_{m=0}^{n} \sum_{\nu=1}^{2} ({}_\nu x_{n,l}^m)({}_\nu x_{n,l}^m)}_{\equiv \mathcal{Q}_{n,l}} \tag{3.1.1}$$

where x represents numbers related to the spectral expansion of a given field. The summation indices l, n, m, and ν refer to model level, total wavenumber, zonal wavenumber, and real/imaginary part of the coefficients, respectively. Clearly, $\mathcal{Q}_{n,l}$ represents the contribution of the field (at total wavenumber n, and model level l) to the complete sum $\mathcal{Q}$. For the spectral decomposition of the total variance in $\mathbf{P}_\zeta^a$ (of Fig. 1) the specification:

$$({}_\nu x_{n,l}^m) = \left[\mathrm{var}({}_\nu \zeta_{n,l}^m) \right]^{1/2} = (\mathbf{P}_\zeta^a)_{ii}^{1/2} \tag{3.1.2}$$

is made (x is set to the square–root of the diagonal elements of $\mathbf{P}_\zeta^a$, after proper reordering), so that $\mathcal{Q}$ takes on the value of 1.0449×10^{-11} s^{-2} (see above), since $\mathcal{Q}$=trace($\mathbf{P}_\zeta^a$), and $\mathcal{Q}_{n,l}$ is referred to as the spectral decomposition of the total variance. This spectral decomposition is shown in Fig. 2. It is clearly evident from Fig. 2 that the spectral variance decomposition is strongly scale dependent, so that this spectrum is very different from a white spectrum. Fig. 2 may also be compared with Fig. 12 of Bouttier et al. (1997) which indicates that the vorticity variances in the IFS background formulation are also strongly scale–dependent,

with a peak around total wavenumber 20 to 40 (depending on model level). Additional information on $\mathbf{P}^a_\zeta$ (e.g., on off–diagonal elements; see also below) may be found in Ehrendorfer and Bouttier (1998b).

3.2 QG/EKF SINGULAR VECTORS

The leading SV computed with QG dynamics according to eq. (1.1), on the basis of the full analysis error covariance matrix (introduced in section 3.1) as constraint at the initial time, is shown in Fig. 3 at initial time (for an optimization time of 48 hours). The final norm used for this computation is total energy (TE) as appropriate for the discrete formulation of the QG model (see, Ehrendorfer 1998a). It is remarkable that this SV is located over the large–variance region (data void) in the southern Atlantic. On the other hand, leading SVs are found to be located preferably in regions offering the possibility for growth due to dynamic instabilities, when total energy is used at both initial and final times (denoted TE/TE SVs). Also, it is evident that this QG/EKF SV has much larger amplitude in the top model level than in the lowest model level (which is related to the vertical variance distribution; see Fig. 1). Also, for this QG/EKF SV much of its total energy is, at the initial time, found around total wavenumber 10, while for the TE/TE SVs, total energy is found at small scales initially and larger scales at the final time.

Given that the set of SVs $\mathbf{Z}_0$ satisfies eq. (1.1), it is possible to represent $\mathbf{P}^a$ as:

$$\mathbf{P}^a = \mathbf{Z}_0 \mathbf{Z}_0^{\mathrm{T}} \tag{3.2.1}$$

(see also, Ehrendorfer 1998b). Obviously, (3.2.1) represents a "square–root" decomposition of $\mathbf{P}^a$; the specific form (3.2.1) will be referred to as SV decomposition, as it decomposes $\mathbf{P}^a$ in terms of the initial–time SVs $\mathbf{Z}_0$. The significance of the SV–decomposition (3.2.1) is that it is not the eigendecomposition of $\mathbf{P}^a$, but rather that it evolves (under tangent–linear dynamics) into the *eigendecomposition* of the forecast error covariance matrix (see also, Ehrendorfer and Tribbia 1997). In other words, if $\mathbf{P}^a$ is, as in (3.2.1), represented in terms of the initial SVs, and if this representation is truncated to a representation in terms of N SVs, this truncated representation will lead, when time–evolved, to the eigenstructure (represented by N eigenvectors) of the forecast error covariance matrix. Obviously, for this reason, the representation (3.2.1) is an attractive candidate for specifying a square–root of $\mathbf{P}^a$. Specification of such a square–root is, for example, necessary, when a sample (i.e., initial ensemble) consistent with the $\mathbf{P}^a$ covariance information is to be generated (see also section 3.3).

The amount of variance described by retaining the leading N SVs in the SV–decomposition (3.2.1) is shown in a cumulative way as the solid curve in Fig. 4 for $\mathbf{P}^a_\zeta$ introduced in section 3.1. The figure also shows the variance reconstruction through the *eigenvectors* of $\mathbf{P}^a_\zeta$ (dashed curve). Both curves are normalized by the total variance of 1.0449×10^{-11} s^{-2} (see above). Clearly, the eigenspectrum curve is steeper; however, the slower SV–decomposition evolves into a similarly steep curve at the optimization time. In Fig. 4, 100 (500) initial–time SVs $\mathbf{Z}_0$ account for 17% (65%) of the initial variance, and describe (at optimization time) 56% (91%) of the forecast error variance.

3.3 QG ENSEMBLE INTEGRATIONS BASED ON $\mathbf{P}^a_\zeta$

Knowledge of the analysis error covariance $\mathbf{P}^a$ is necessary for the process of generating realistic initial perturbations in the context of ensemble prediction, since $\mathbf{P}^a$ contains important information about the initial–time pdf. Specifically, perturbations may be generated that are consistent with the knowledge of the initial–time probability density function (pdf) in terms of its first and second moments.

Given $\mathbf{P}^a$, as well as its decomposition (3.2.1), the possibility of generating an arbitrary number (say M) of initial perturbations to be used in ensemble prediction given a fixed number (say N) of SVs was studied here in the context of the QG model (i.e., the M perturbations are evolved with QG dynamics). The time–evolved ensemble of size M is subsequently used to estimate statistics of the time–evolved pdf.

The approach tested here is closely related to the technique for generating initial perturbations, given a set of N SVs, as it is presently used operationally at ECMWF (see, Molteni et al. 1996). However, the approach described here is explicitly based on a sampling process from a multivariate normal distribution (see also, Ehrendorfer 1998b), which is not the case for the rotational technique described by Molteni et al. (1996). The sampling process described here, called SV–based Monte Carlo (MC) technique, is based on the fact that a random vector $\mathbf{x}$ with multivariate normal pdf with mean $\mathbf{x}^c_0$ and covariance structure $\mathbf{V}$ is obtained as:

$$\mathbf{x} = \mathbf{x}^c_0 + \mathbf{V}^{1/2}\mathbf{q} \qquad \rightarrow \qquad \mathbf{x} \sim \mathcal{N}(\mathbf{x}^c_0, \mathbf{V}) \,, \tag{3.3.1}$$

where $\mathbf{q}$ is multivariate standard normal:

$$\mathbf{q} \sim \mathcal{N}(0, \mathbf{I}) \,. \tag{3.3.2}$$

Here $\mathbf{V}^{1/2}$ denotes a square–root of the covariance structure $\mathbf{V}$ (to be interpreted as the analysis error covariance matrix), and the notation "$\sim \mathcal{N}$" is used to denote "normally distributed" with parameters as

indicated (e.g., Anderson 1958). The symbol $\mathbf{I}$ denotes the identity matrix, so that the random vector $\mathbf{q}$ is multivariate standard–normal.

Given (3.3.1), the SV–based MC technique exploits the SV–decomposition of $\mathbf{P}^a$, possibly truncated to N SVs, to provide a square–root of $\mathbf{P}^a$ as needed in (3.3.1), in the process of generating perturbed states $\mathbf{x}$:

$$(\mathbf{P}^a)^{1/2} = \mathbf{Z}_0^{(N)}, \tag{3.3.3}$$

where $\mathbf{Z}_0^{(N)}$ indicates the matrix containing as columns the N SVs available. Consequently, the set of M perturbed initial states is generated, by combining (3.3.1) and (3.3.3), as:

$$\mathbf{x}_i = \mathbf{x}_0^c + \mathbf{Z}_0^{(N)}\mathbf{q}_i \qquad i = 1, 2, ..., M \quad \Rightarrow \quad \mathbf{x} \sim \mathcal{N}\Big(\mathbf{x}_0^c, (\mathbf{P}^a)^{(N)}\Big), \tag{3.3.4}$$

where $\mathbf{q}_i$ is a realization from $\mathcal{N}(0, \mathbf{I})$, and as indicated in (3.3.4), the resulting set $\mathbf{x}_i$ is a sample from a multivariate normal pdf with parameters as written in (3.3.4). Specifically, the covariance structure of these perturbed states is consistent with the knowledge about $\mathbf{P}^a$ as contained in the N leading SVs. It becomes also clear that the process (3.3.4) assumes explicitly that the analysis errors are normally distributed, as the sampling proceeds from a normal pdf. Referring to the introductory discussion in section 1, this process again relies on the decomposition (3.2.1) that evolves into the eigendecomposition of the forecast error covariance matrix (under linear dynamics). Since the M–member ensemble is evolved nonlinearly, it appears to be possible to take the SV properties into the nonlinear regime.

By arranging the deviations $\mathbf{x}_i - \mathbf{x}_0^c$ in (3.3.4) as the M columns of the matrix $\mathbf{X}$ (and similarly forming the M columns of the $N \times M$ matrix $\mathbf{Q}$ through the vectors $\mathbf{q}_i$), it becomes obvious that an ensemble of size M generated by (3.3.4) has – by construction – a sample covariance structure of:

$$\hat{\mathbf{P}}^a \equiv \frac{1}{M}\mathbf{X}\mathbf{X}^{\mathrm{T}} = \Big(\mathbf{Z}_0^{(N)}\Big)\Big(\frac{1}{M}\mathbf{Q}\mathbf{Q}^{\mathrm{T}}\Big)\Big(\mathbf{Z}_0^{(N)}\Big)^{\mathrm{T}} \to \Big(\mathbf{Z}_0^{(N)}\Big)\Big(\mathbf{Z}_0^{(N)}\Big)^{\mathrm{T}} \equiv (\mathbf{P}^a)^{(N)} \qquad \text{as} \qquad \frac{1}{M}\mathbf{Q}\mathbf{Q}^{\mathrm{T}} \to \mathbf{I} \tag{3.3.5}$$

where the arrows indicate the limits that are approached for increasing M. Clearly, $\hat{\mathbf{P}}^a$ is (in the limit of large M) the version of $\mathbf{P}^a$ (see eqs. (3.2.1) and (3.3.3)) that is truncated in terms of the N available SVs, denoted as $(\mathbf{P}^a)^{(N)}$. Consequently, the set of perturbed states $\mathbf{x}_i$ generated through (3.3.4) is a set of M realizations from $\mathcal{N}(\mathbf{x}_0^c, (\mathbf{P}^a)^{(N)})$. The sampling process (3.3.4) combined with the time evolution of such an ensemble is referred to as SV–based MC method, since it combines random sampling (i.e., the MC approach) with analysis error covariance information provided through SVs. Note again that this technique leading to the set of perturbations $\mathbf{X}$, compactly written in the form $\mathbf{X} = \mathbf{Z}_0^{(N)}\mathbf{Q}$, bears a strong relationship to the rotation of available SVs (see, Molteni et al. 1996) as presently performed operationally at ECMWF, since $\mathbf{Z}_0^{(N)}\mathbf{q}_i$ may obviously be interpreted as a (statistically–based) linear combination of the available SVs (note again that the vectors $\mathbf{q}_i$ are not specified to be standard–normal in the ECMWF rotation technique).

Clearly, in the purely linear situation, it is only necessary to evolve N SVs over time in order to obtain the eigenstructure of the forecast error covariance matrix. However, as nonlinearities become more important, sampling along various different directions at the initial time, as achieved by taking $M > N$ in the SV–based MC method, potentially allows for a more accurate representation of the time–evolving forecast error covariance structure. Or, put differently, increasing the ensemble size M for given initial pdf information (i.e., fixed N) should be expected to lead to a more accurate representation of the time–evolving forecast error covariances, as soon as nonlinear effects become important. Note that the SV–based MC method allows independent specification of M and N, and that this technique may also be interpreted as sampling from a multivariate normal pdf, where the sampling process "sees" only that part of $\mathbf{P}^a$ that is explained by the N SVs available.

The SV–based MC method was tested in the QG model, on the basis of the analysis error covariance matrices $\mathbf{P}_\zeta^a$ available from the QG/EKF. It was found that small M and N (e.g., equal to 100) are sufficient for very accurate estimation of the time–evolving mean (for 96h–integrations). Similarly, for N=500 (explaining 65% of the initial variance; see above), the 96–hour evolved *variances* are already quite accurate for $M = 100$; the differences found when M is increased to 5000, are recognizeable, but not substantial. However, for the time–evolving *correlations* it appears for $N = 500$ (i.e., for the "coarse–grained" analysis error covariance description) to be beneficial if the ensemble size M is large. As illustrated in Fig. 5, a substantial improvement in the estimated time–evolved (over 96h) correlations occurs, when M is increased from 100 to 5000 (compare panels (a) and (b)). It can also be seen from Fig. 5 that increasing N changes these correlations only very little, which is an indication that most of the relevant initial pdf information is already captured when $N = 500$ (compare panels ((b) and (c)).

It is necessary to mention at this point that $(\mathbf{P}^a)^{(N)}$ (see, eq. (3.3.4)) is "variance–deficient" if the sampling process is carried out as written in (3.3.4), in the sense that it contains only the fraction of total

initial variance described by the first N SVs. In view of the rapid initial growth of the leading N SVs, it is difficult to devise a general rule for the choice of an additional initial scaling paramater. In the experiments described here, no scaling parameter has been applied (see also, Ehrendorfer 1998b).

In concluding this section, Fig. 6 is included to give an indication of the error–growth properties of the QG model, by plotting the trace of the nonlinearly time–evolving forecast error covariance matrix. The results of this figure have been obtained by evolving a moderately large ($M = 500$) ensemble, generated on the basis of (3.3.4), over a period of approximately 15 days. Such ensembles were used to estimate the forecast error covariance matrix at different lead times during the integration process. Here, the different lines correspond to different choices for $(\mathbf{P}^a_\zeta)^{(N)}$ (with $N = 1449$), as they result for different days during the QG/EKF experiment described at the beginning of section 3. It is seen from Fig. 6, that the initially small variances double approximately every 36 hours (the corresponding doubling time for standard deviations is approximately 3 days), which is a reasonably realistic value when compared to error–doubling times in operational models (e.g., Simmons et al. 1995).

3.4 $\mathbf{P}^a_\zeta$ IN THE IFS CONTROL–VARIABLE SPACE

As pointed out in section 2, the QG/EKF represents an exact implementation of the second–order EKF equations at low resolution. It is clear that such an exact implementation is a potentially useful reference when it is desired to assess the performance of EKF implementations with *approximated* equations. Such approximations to the EKF equations seem unavoidable in reasonably high–resolution data assimilation systems, suitable for possible operational implementation. In this case, it is, in principle, possible to judge the form of such approximations against the unapproximated EKF in the context of the T21L3 QG/EKF.

One such approximated form of the EKF equations, called simplified Kalman filter (SKF), has been described by Fisher (1998). It is presently tested in a high–resolution context. One of the assumptions in the SKF concerns the spectrum of the background error covariances in the so–called IFS control variable space (i.e., the preconditioned space in which the variational minimization is carried out; see also Bouttier et al. 1997).

The spectrum of flow–independent (static) background error formulations is, in this space, equal to the spectrum of the identity matrix. In the SKF formulation, the leading part of the background error covariance spectrum is made different from unity by introducing some flow dependence. Within the QG/EKF it was investigated how different the spectrum of the background valid for 19971201/00GMT is from unity (this is the background serving as input into eq. (2.1), when the analysis error covariance matrix discussed in section 3.1 is computed). The control–variable spectrum of the background error is shown in Fig. 7a (lower curve, labeled "spectrum inverse Hessian"). The largest eigenvalue is approximately 5.5, and it can be seen that approximately 20% of the eigenvalues (i.e. 320) are larger than one. Fig. 7b, shows the corresponding cumulative picture, with the lower curve corresponding to the background error covariances. Taking all the eigenvalues into account that are larger than one, allows one to obtain a cumulative variance fraction of approximately 60%.

Carrying out diagnostics similar to this eigenspectrum computation in control–variable space may be a promising way to judge the degree of validity of certain assumptions when the EKF equations are approximated in the process of developing computationally feasible implementations at high resolution.

4. CONCLUDING REMARKS

The implementation of the QG/EKF at the resolution T21/L3 allows for (i) the explicit assessment of the analysis error covariance structures $\mathbf{P}^a$, as well as (ii) use and generation of time/flow–dependent background error covariances $\mathbf{P}^f$ (as predicted with the QG model). Knowledge about $\mathbf{P}^a$ is of primary importance in a predictability context for the realistic generation of perturbations in ensemble prediction. On the other hand, knowledge about $\mathbf{P}^f$ is a necessary to specify the so–called background term in variational data assimilation in a realistic manner.

Several preliminary results obtained with the QG/EKF were discussed in the previous sections. First, as expected, $\mathbf{P}^a$ and $\mathbf{P}^f$ reflect data–rich and data–void areas, and are rather different in structure from assumed flow–independent covariances. Further, the QG/EKF SVs were found to be rather different from SVs based on (for example) total energy at both initial and final times. In terms of reconstructing the analysis error covariance matrix $\mathbf{P}^a$ through the EKF SVs it was found that 100 (500) (out of 1449) SVs account for 17% (65%) of the total initial variance (in the case studied). If a final–time projection operator is applied, these cumulative percentages are increasing when the projected final–time variance is reconstructed.

Ensemble integrations with sampling from $\mathbf{P}^a$ (truncated in their representation to N SVs; see eq. (3.2.1) and (3.3.3)), indicate that moderate ensemble sizes lead to good estimates of time–evolved mean and variances, but that increased ensemble sizes M are improving the estimates for time–evolved correlations considerably. The investigation of a selected QG/EKF (vorticity) background error covariance matrix in the IFS control–variable space shows that the flow–dependent eigenspectrum is rather different from the

unit spectrum used in the background term in the variational preconditioning: approximately 20% of the eigenvalues are larger than one (1449 degrees of freedom).

The QG/EKF software developed should be relatively easily adaptable to the use of a different dynamical model, or to an upgrade of the resolution to T42. Also, it should be possible to approximate various steps (e.g., the prediction step) along the lines of the simplified Kalman filter (see also, Fisher 1998). It will be necessary to study in more detail the impact of observations (density and type) on, for example, the required model error specification, and on the overall equilibrium variance levels obtained, as well as on the specific properties of SVs constrained initially with the so–obtained $\mathbf{P}^a$ matrices. More detailed results in this respect will also be necessary to interface background error covariances from the QG/EKF with a higher–resolution data assimilation scheme, and to understand at a deeper level the modifications of singular vectors when analysis error covariances are used to constrain them at initial time.

Acknowledgment. Most of this research was carried out during a one–year visit of the author to the European Centre for Medium–Range Weather Forecasts (ECMWF). This visit was funded by ECMWF.

REFERENCES

Anderson, T.W., 1958: An introduction to multivariate statistical analysis. Wiley, 374 pp.

Bouttier, F., J. Derber, and M. Fisher, 1997: The 1997 revision of the J_b term in 3D/4D-Var. ECMWF Technical Memorandum No. 238, 54pp.

Burgers, G., P.J. van Leeuwen, and G. Evensen, 1998: Analysis scheme in the ensemble Kalman filter. *Monthly Weather Review,* **126**, 1719–1724.

Cohn, S.E., 1997: An introduction to estimation theory. *Journal of the Meteorological Society of Japan,* **75 (1B)**, 257–288.

Courtier, P., 1997: Variational methods. *Journal of the Meteorological Society of Japan,* **75 (1B)**, 211–218.

Courtier, P., E. Andersson, W. Heckley, J. Pailleux, D. Vasiljević, M. Hamrud, A. Hollingsworth, F. Rabier, and M. Fisher, 1998: The ECMWF implementation of three–dimensional variational assimilation (3D-Var). I: Formulation. *Quarterly Journal of the Royal Meteorological Society,* **124**, 1783–1807.

Ehrendorfer, M., 1998a: Energy norms in the T21L3 Marshall/Molteni quasigeostrophic model. ECMWF Research Department memorandum. 28pp.

Ehrendorfer, M., 1998b: Prediction of the uncertainty of numerical weather forecasts: problems and approaches. Proceedings ECMWF Workshop on Predictability, 20 – 23 October 1997, 27–101.

Ehrendorfer, M., and F. Bouttier, 1998a: An explicit low–resolution extended Kalman filter based on quasi-geostrophic dynamics: technical description. ECMWF Research Department memorandum. 24pp.

Ehrendorfer, M., and F. Bouttier, 1998b: An explicit low–resolution extended Kalman filter: implementation and preliminary experimentation. ECMWF Technical Memorandum No. 259, 21pp.

Ehrendorfer, M., and J.J. Tribbia, 1997: Optimal prediction of forecast error covariances through singular vectors. Journal of the Atmospheric Sciences, **54**, 286–313.

Epstein, E.S., 1969: Stochastic dynamic prediction. *Tellus,* **21**, 739–759.

Fisher, M., 1998: Development of a simplified Kalman filter. ECMWF Technical Memorandum No. 260, 16pp.

Houtekamer, P.L., and H.L. Mitchell, 1998: Data assimilation using an ensemble Kalman filter technique. *Monthly Weather Review,* **126**, 796–811.

Ide, K., P. Courtier, M, Ghil, and A.C. Lorenc, 1997: Unified notation for data assimilation: operational, sequential and variational. *Journal of the Meteorological Society of Japan,* **75, 1B**, 181–189.

Marshall, J., and F. Molteni, 1993: Towards a dynamical understanding of planetary–scale flow regimes. *Journal of the Atmospheric Sciences,* **50**, 1792–1818.

Molteni, F., R. Buizza, T.N. Palmer, and T. Petroliagis, 1996: The ECMWF ensemble prediction system: methodology and validation. Quarterly Journal of the Royal Meteorological Society, **122**, 73–119.

Palmer, T.N., R. Gelaro, J. Barkmeijer, and R. Buizza, 1998: Singular vectors, metrics, and adaptive observations. *Journal of the Atmospheric Sciences,* **55**, 633–653.

Rabier, F., J.-F. Mahfouf, M. Fisher, et al., 1997: Recent experimentation on 4D-VAR and first results from a Simplified Kalman Filter. ECMWF Technical Memorandum No. 240, 42pp.

Simmons, A.J., R. Mureau, and T. Petroliagis, 1995: Error growth and estimates of predictability from the ECMWF forecasting system. *Quarterly Journal of the Royal Meteorological Society,* **121**, 1739–1771.

Todling, R., S.E. Cohn, and N.S. Sivakumaran, 1998: Suboptimal schemes for retrospective data assimilation based on the fixed–lag Kalman smoother. *Monthly Weather Review,* **126**, 2274–2286.

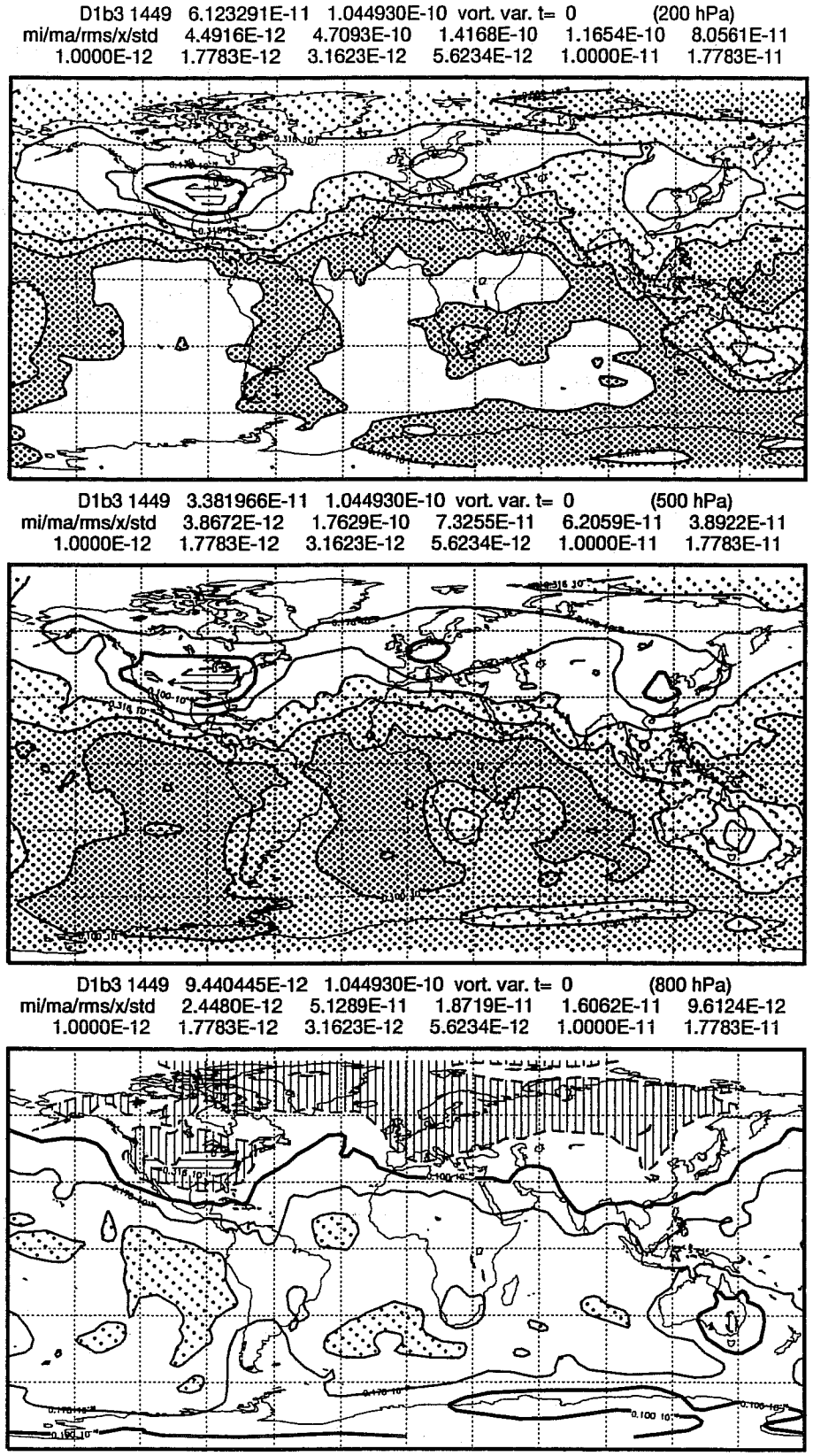

Fig. 1. Vorticity variances at the three model levels (200 hPa, 500 hPa, 800 hPa; from top to bottom) in physical space in units of s^{-2} for the analysis error covariance matrix $\mathbf{P}_\zeta^a$ valid at 19971201/00GMT. The heavy contour denotes the value 10^{-11} s^{-2}. The same contours and shading conventions are used in all panels. Darker shading corresponds to larger variances, hatching to low variances. Unshaded regions within light (dark) shading indicate high (low) variances.

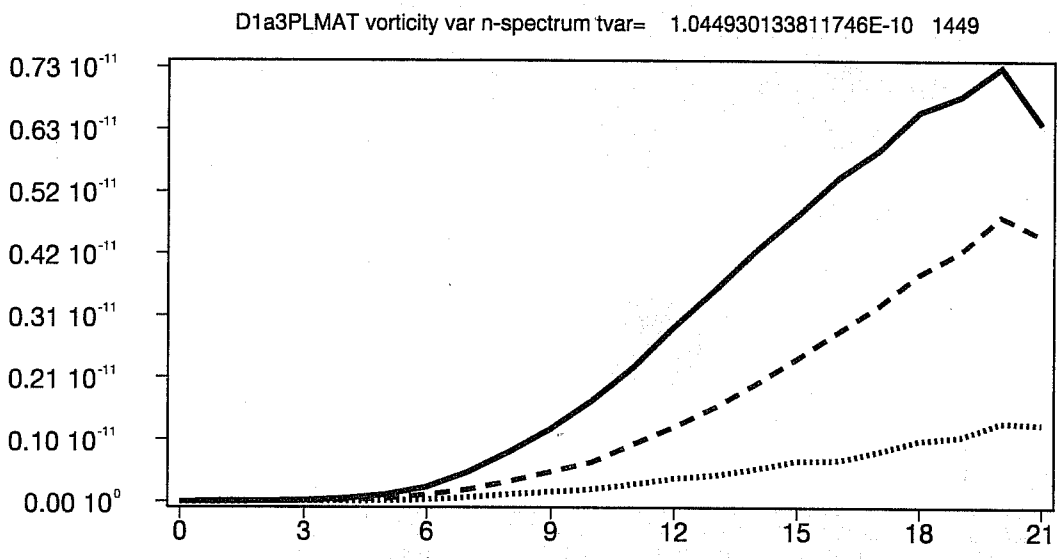

Fig. 2. Spectral decomposition of the total vorticity variance of 1.0449×10^{-11} s^{-2} contained in $\mathbf{P}^a_\zeta$ (valid at 19971201/00GMT), as described in section 3.1, as a function of total wavenumber n. Solid/dashed/dotted lines are for top/middle/bottom model levels. Note that analysis error vorticity variances are strongly scale–dependent.

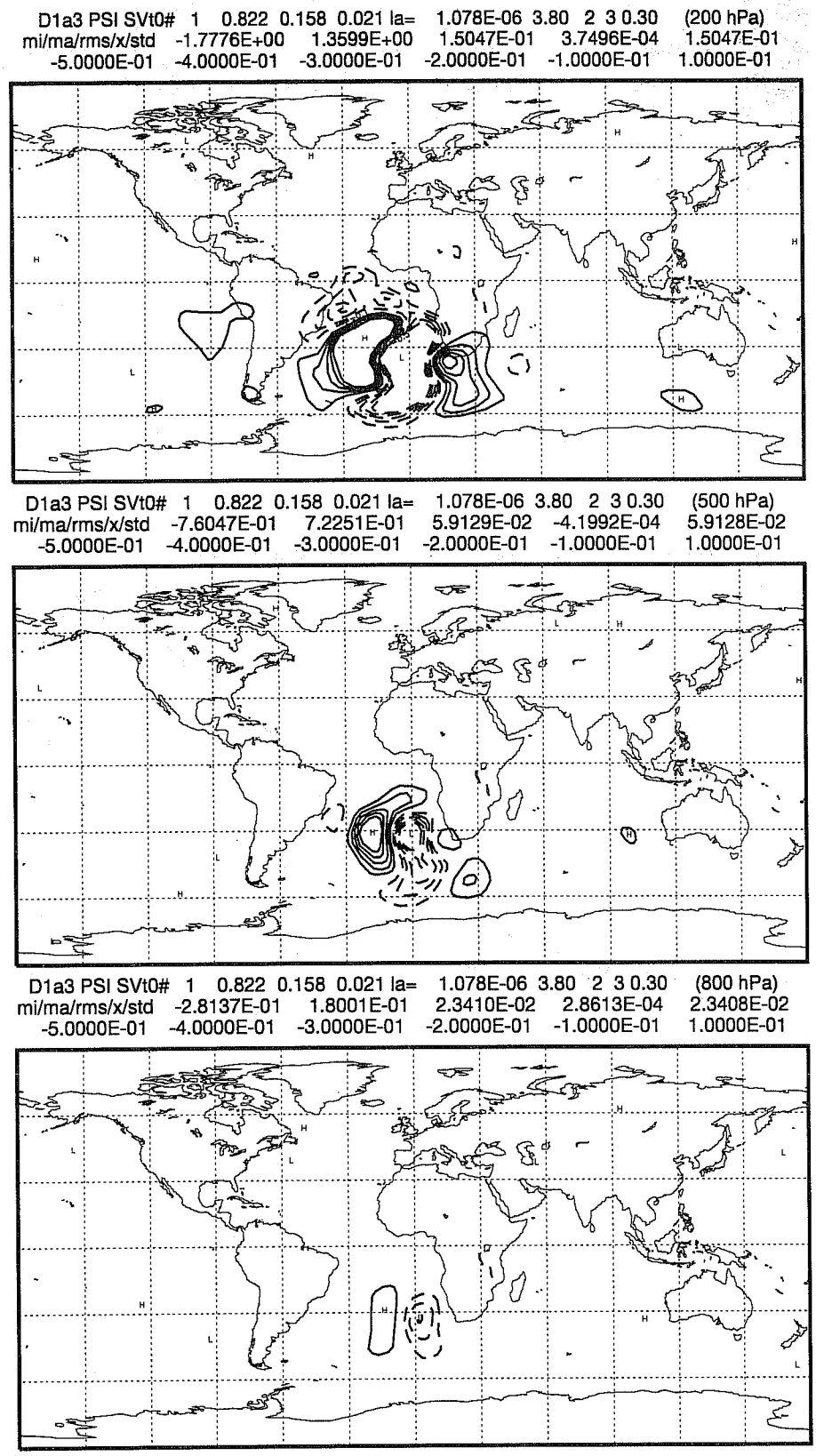

Fig. 3. The leading EKF singular vector at initial time, at the three model levels, computed with quasi-geostrophic dynamics over the 48–hour optimization interval from 19971201/00GMT to 19971203/00GMT. The initial constraint is defined by $\mathbf{P}_\zeta^a$ (see Fig. 1), the final norm is total energy. The singular vector is scaled to total energy equal one and is plotted in terms of a streamfunction perturbation. The same contour interval of 0.1 is used in all panels.

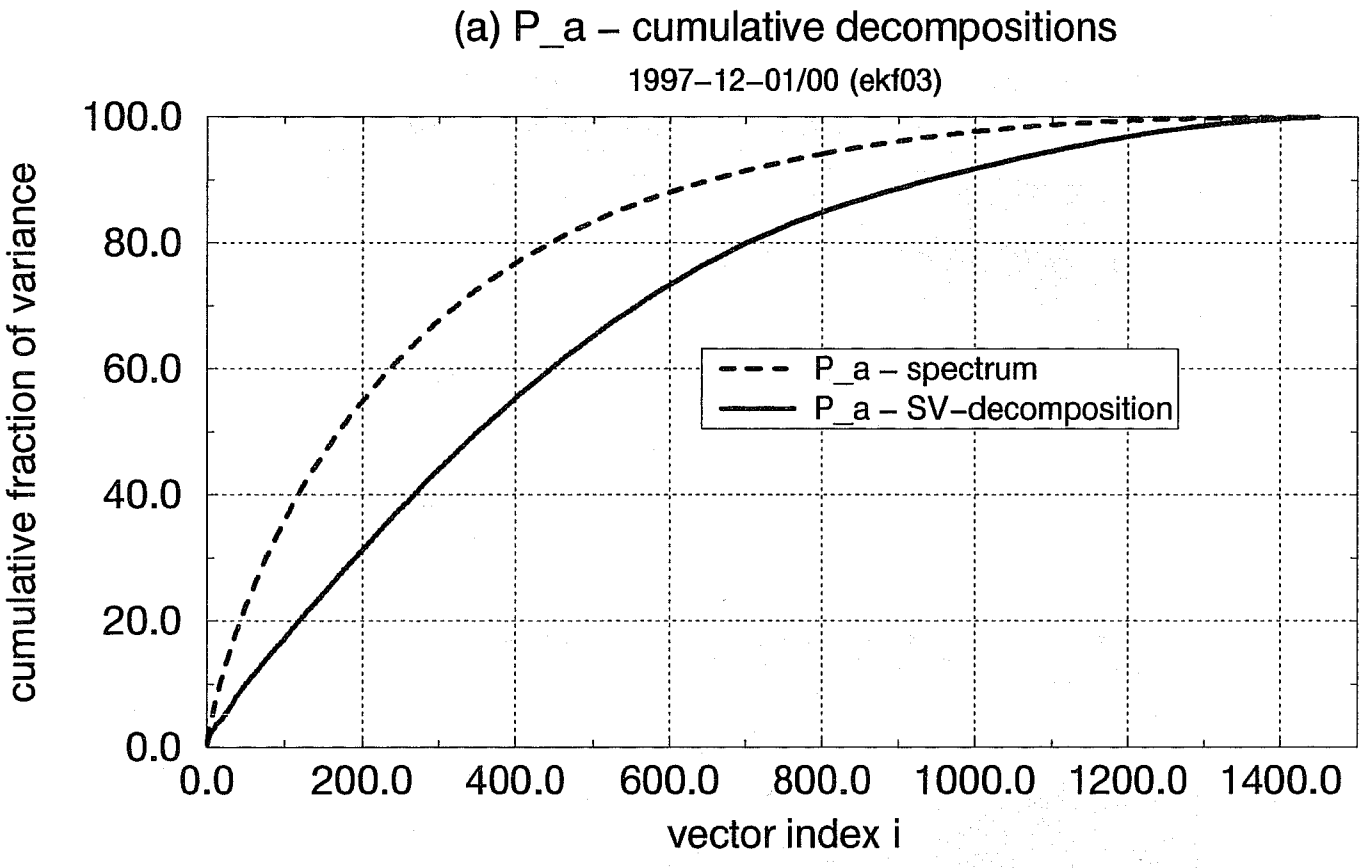

Fig. 4. Cumulative decomposition of vorticity analysis error covariance matrix $\mathbf{P}_\zeta^a$ (valid at 19971201/ 00GMT), in terms of cumulative fractions of variance (in percent), as a function of the number of vectors used in the decomposition. The dashed curve shows the eigenspectrum of $\mathbf{P}_\zeta^a$, the solid curve shows its SV–decomposition (see eq. (3.2.1)) in terms of the initial–time 48–hour optimized EKF singular vectors $\mathbf{Z}_0$ (computed with total energy at the final time).

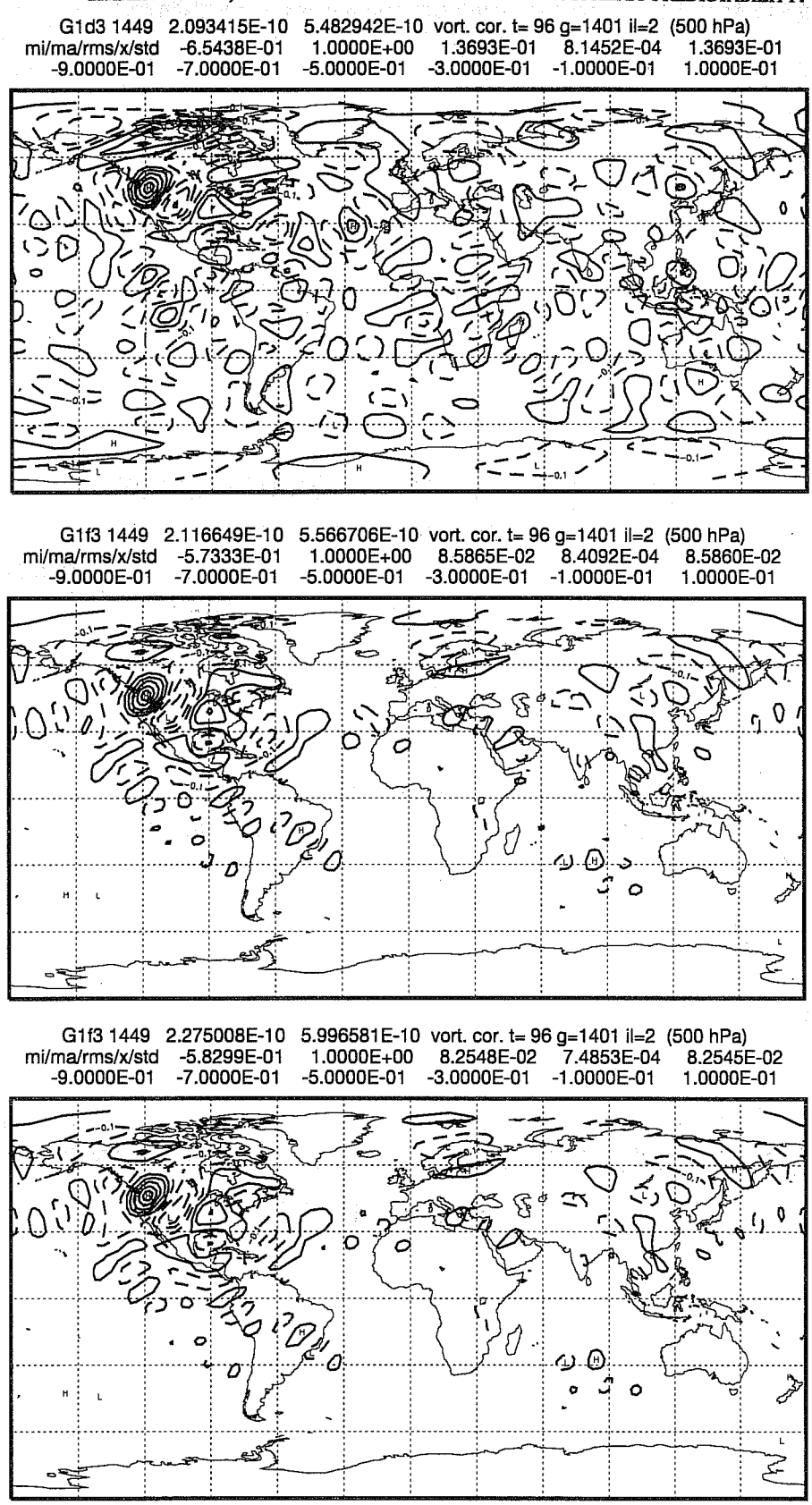

Fig. 5. Time–evolved correlation structures as estimated from time–evolved (with the QG model) ensembles computed on the basis of the SV–based MC method. Shown is the correlation of a grid point over North America at 500 hPa, with all other grid points at that model level. The integration interval is the 96–hour period starting on 19971204/00GMT, where the corresponding analysis error covariance matrix $\mathbf{P}^a_\zeta$ is used in the sampling process (3.3.4). The panels differ in the choice of the values N and M (see section 3.3): (a) N=500, M=100; (b) N=500, M=5000; (c) N=1449; M=5000. Note the improvement in the estimated correlations between (a) and (b), and the very small differences between (b) and (c).

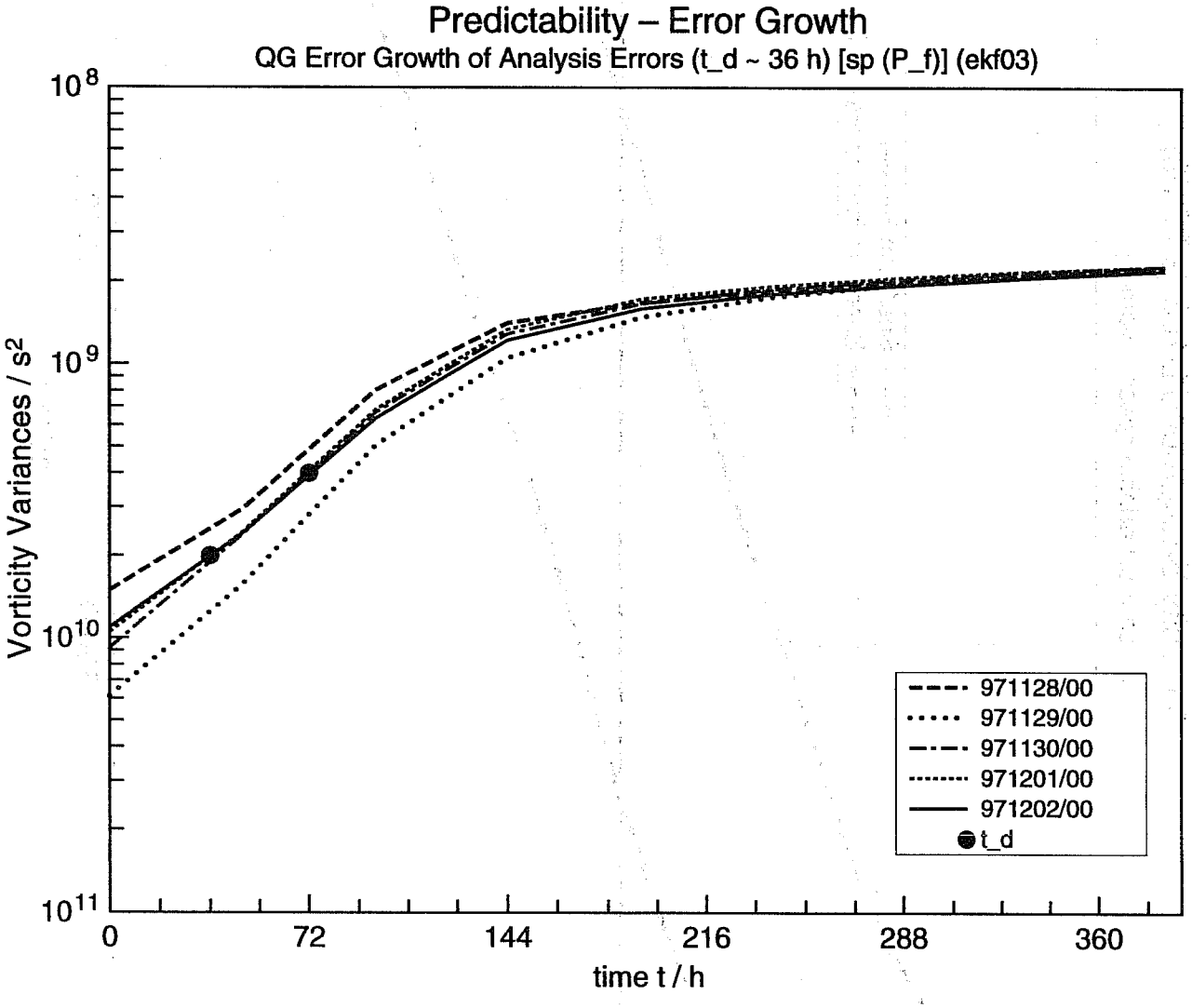

Fig. 6. Predictability error growth curves in the QG model. Shown is the time evolution of the trace of the forecast error covariance matrices, over approximately 15 days, for five different starting dates. For each curve, an initial ensemble with M = 500 was generated on the basis of (3.3.4), with the relevant $\mathbf{x}_0^c$ and $\mathbf{P}_\zeta^a$, and subsequently evolved nonlinearly over time. As indicated, the variance doubling time is approximately 36 hours for small variances. Note the logarithmic ordinate.

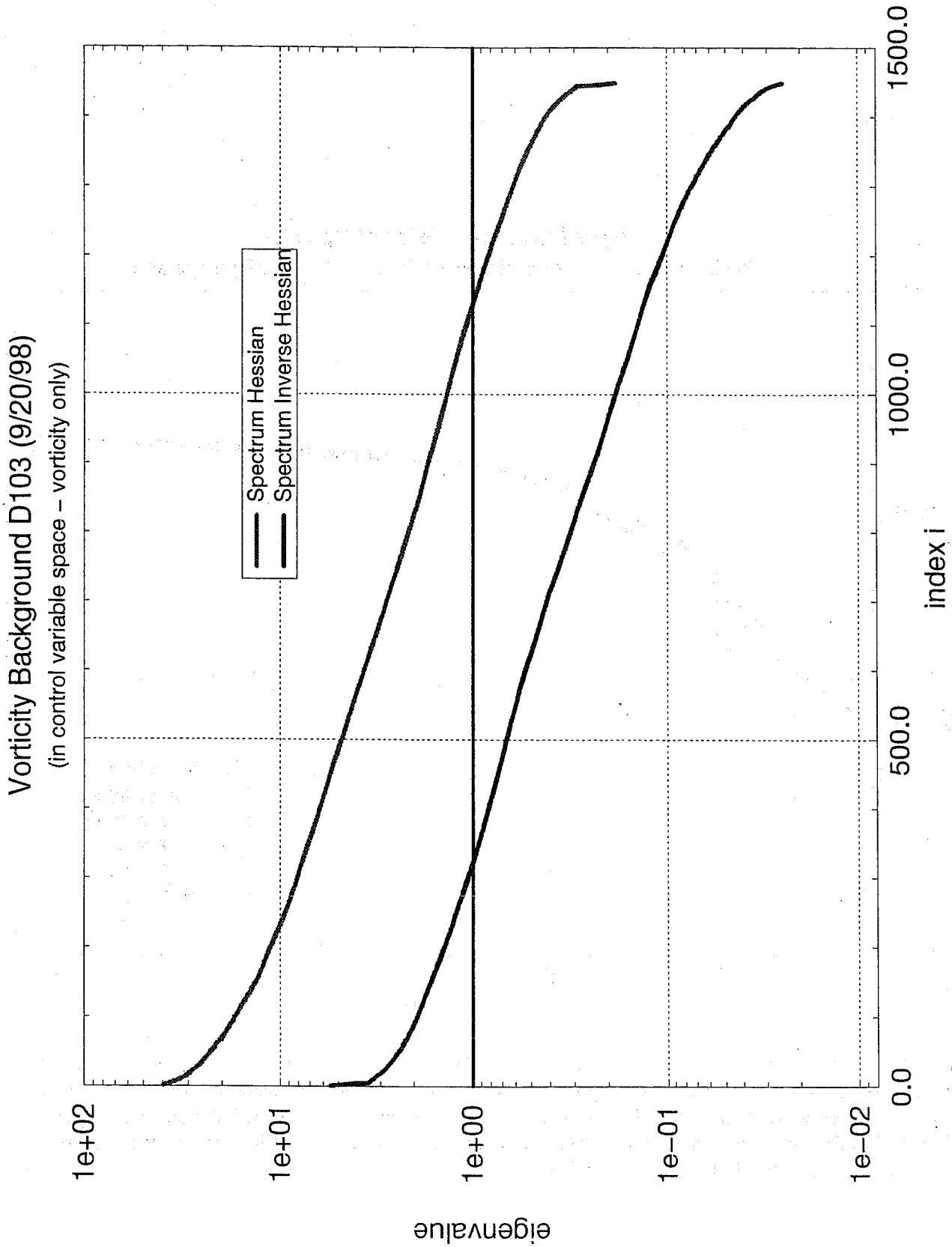

Fig. 7a. The spectrum of the background error covariance matrix valid for 19971201/00GMT in the IFS control–variable space (lower curve); the upper curve is the spectrum of the inverse of this covariance matrix (i.e., the spectrum of the control–variable space background Hessian). Note that, consequently, the largest eigenvalue of lower curve is equal to the inverse of the smallest eigenvalue of the upper curve (with analogous inverse relationships for the other eigenvalues). Approximately 320 of the eigenvalues of the background are greater than one (i.e., 22%).

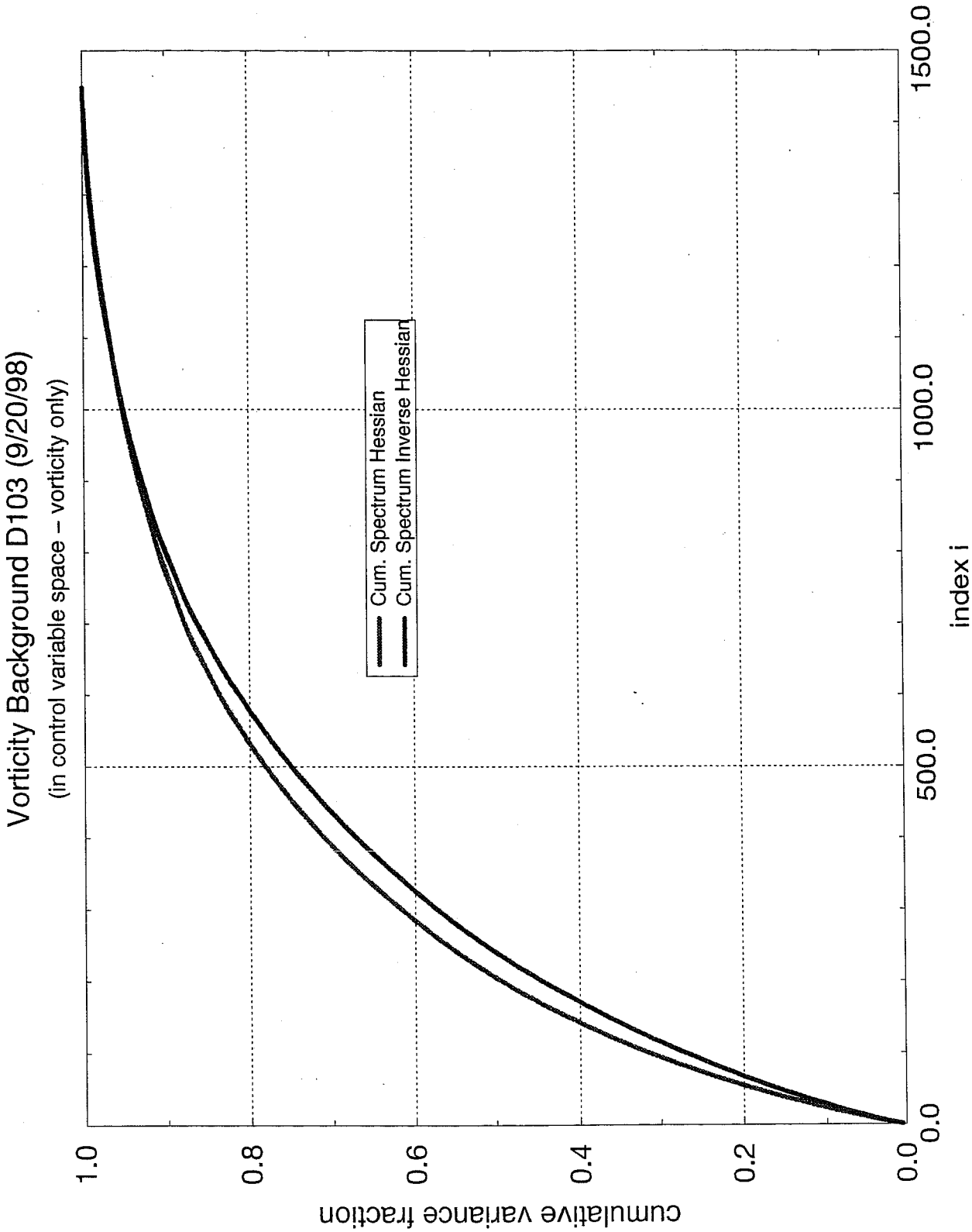

Fig. 7b. Cumulative spectra for the curves of Fig. 7a (upper curve Hessian; lower curve inverse Hessian). The cumulative variance fraction accounted for by the eigenvalues larger than one is approximately 60%.